Solar Energy 239 (2022) 170–178

Contents lists available at ScienceDirect

Solar Energy

journal homepage: www.elsevier.com/locate/solener

Parabolic trough field control utilizing all sky imager irradiance data – A comprehensive robustness analysis

Tim Kotzab [a,*], Sebastian Müllner [a], Tobias Hirsch [a], Kareem Noureldin [a], Bijan Nouri [b], Mark Schmitz [c], Luis Fernando Zarzalejo [d], Robert Pitz-Paal [e]

[a] German Aerospace Center (DLR), Institute of Solar Research, Wankelstrasse 5, 70563 Stuttgart, Germany
[b] German Aerospace Center (DLR), Institute of Solar Research, Ctra de Senes s/n km 4, 04200 Tabernas, Spain
[c] TSK Flagsol Engineering GmbH, Anna-Schneider-Steig 10, 50678 Cologne, Germany
[d] CIEMAT Energy Department – Renewable Energy Division, Av. Complutense 40, 28040 Madrid, Spain
[e] German Aerospace Center (DLR), Institute of Solar Research, Linder Höhe, 51147 Cologne, Germany

ARTICLE INFO

Keywords:
Parabolic trough power plant
Solar field control
Robustness analysis
Virtual solar field
Irradiance maps
Irradiance forecast

ABSTRACT

Parabolic trough (PT) power plants focus the sun's irradiation onto an absorber tube using collector mirrors to increase the temperature of the heat transfer medium (HTF). In the power plant, the HTF is used to generate electricity. To heat up the HTF, PT solar fields are set up in large areas and pipes are used to distribute the HTF in the solar field. The control system adjusts the temperature by changing the mass flow into the solar field and the focusing of the individual collectors. Transient conditions such as cloud passage are the main challenge for the system. State of the art control schemes use information from a few irradiation measuring points in the solar field. These measurement points are precise for the individual location but cannot accurately represent the irradiation situation in the whole solar field. In this paper, a control system that uses spatially resolved irradiation information from all sky imager systems is investigated.

First, the control system was developed and tested in various simulation runs under ideal conditions. The focus of this work is to investigate the robustness of the control concept under non-ideal conditions. For this purpose, the simulation conditions are adapted to real situations and the behavior of the control system is analyzed.

A robust behavior of the control system is shown in the simulations under different non-ideal scenarios. Overall, an improvement in electrical yield of 1.4% can be achieved compared to a reference without access to spatially resolved irradiance data.

1. Introduction

Generating solar electricity from the sun can be divided into the two systems of photovoltaics (PV) and concentrating solar power (CSP). Together, these two systems have reached a global installation of 714 GW (IRENA 2021) by the end of 2020. The larger part of 707.5 GW represents the PV systems compared to the CSP systems with 6.5 GW (IRENA 2021).

PV and CSP systems use solar irradiation to generate electricity. In order to be able to produce the electricity even in times of low irradiation or at night, storage systems have to be used. When using storage, CSP systems with thermal energy storages (TES) show price advantages over PV systems with batteries (Cole and Frazier 2020, Schöniger et al. 2021). Goal of the solar installation in CSP systems is to get the HTF to the design outlet temperature and to collect as much solar energy as possible. This study deals with the control of PT solar power plants. PT solar power plants are large thermal systems that use parabolic mirrors to focus solar irradiation onto an absorber tube in the focal line. Only direct normal irradiance (DNI) can be used for focusing. Commercial PT solar power plants are divided into individual sub-fields with many loops. Valves at the inlet of each loop are used to hydraulically balance the field in a way that each loop receives approximately the same mass flow at design conditions. Only a few plants use control valves at the inlet of each loop whereas most installations are equipped with manual valves. Usually, these valves are used for hydraulically trimming the field during commissioning. This paper refers to such a system with manual valves and fixed valve openings.

Main control tasks in the solar field are the mass flow control and the

* Corresponding author.
E-mail address: tim.kotzab@dlr.de (T. Kotzab).

https://doi.org/10.1016/j.solener.2022.04.059
Received 13 August 2021; Received in revised form 30 March 2022; Accepted 26 April 2022
Available online 13 May 2022

individual collectors' focus control. The goal is to adapt the mass flow in a way that the collectors always focus at 100% to collect the maximum solar energy, while not exceeding the required outlet temperature. If the mass flow is distributed equally among all loops, the focusing and temperature can well be kept constant during clear sky conditions. Challenges occur in transient conditions such as passing clouds. In these situations, shadowed collectors have too much mass flow and the outlet temperature drops, whereas unshaded ones can have too little mass flow and may overheat. If overheating occurs, collectors are moved out of focus to prevent damage to the components and degradation of the HTF. It is the task of a good control concept to find a balance between maintaining high field outlet temperatures and harvesting a high fraction of the available solar energy. An overview of possible control systems is described in Camacho et al. (2007a) and Camacho et al. (2007b).

Solar collector assemblies (SCAs) track the sun in order to focus the DNI on the absorber pipe. Each SCA has its own controller and a focus and defocus strategy (Wittmann et al. 2009). Temperature setpoints are calculated for each SCA and if it is exceeded, the SCAs are automatically moved slightly out of focus. This also acts as a safety measure to avoid damages caused by excessively high temperature gradients. Another part of the SCA focus and defocus strategy is systematic dumping if the overall irradiation is too high or if the TES is fully charged. In this case of dumping, the focus of the individual collectors is reduced depending of the operating strategy.

In the solar field, the mass flow is driven by the pump at the entrance and controlled depending on the temperature and the focus in the solar field. Control parameters can be calculated adaptively using the solar field performance parameters. These are classically used in proportional-integral-derivative (PID) controllers (Zunft 1995, Barcia et al. 2015). By using a feedforward (FF) control, a theoretical mass flow can be calculated for the current DNI (Zunft 1995). Extended control concepts such as model-predictive-control (MPC) are described in (Stuetzle et al. 2004). However, control concepts with PID controllers and FF are mainly used in commercial solar fields. State-of-the-art-control systems use the information of a few pyrheliometers to calculate the required mass flow for the solar field. These few measuring points in the solar field cannot provide a precise measurement of the DNI irradiance in cloudy situations. This leads to inaccuracies in the mass flow calculation. A control system, which receives DNI information from a camera system (Wilbert et al. 2018) has access to better information about the DNI. This camera system uses all-sky imagers (ASI) to detect clouds and calculate spatially and temporally resolved DNI maps. In this paper a control system is investigated, which uses the spatially and temporally resolved DNI maps. The first developments in this system are described in (Noureldin 2018, Schlichting 2018). By using the average DNI in the solar field, calculated from the DNI maps instead of a few pyrheliometers first improvements could theoretically be achieved. Another development step was the classification of the irradiation situation based on the DNI maps. As a result, the controller parameters for the respective irradiation class could be further improved. In the further development in (Müllner 2020), only solar field performance parameters are used, instead of specific solar field design curves. Thus, the control system can be easily applied to any solar field.

In simulation studies, control systems cannot be tested precisely as in the real application. Aim of this study is a robustness analysis of the control system. Here, a stable behavior of the system under different situations is to be guaranteed. With this robustness analysis, occurring uncertainties in the real system are simulated and investigated in a complex simulation tool. First robustness simulations are performed in (Nouri et al. 2020). Uncertainties in DNI maps can occur in camera system calculations. These uncertainties were simulated and the control system was improved. In this paper, the robustness analyses are extended by simulated scenarios which can occur in real solar fields, like soiling or varying inlet temperature.

The simulation tool Virtual Solar Field (VSF) is used for the simulations (Noureldin 2018). VSF represents a complete solar field. By using spatially resolved DNI maps, transient conditions can be simulated as on a real solar field. This allows a comprehensive robustness analysis to be performed with realistic situations.

In the following sections, the camera system used for generating the DNI maps and the simulation tool VSF are presented. Afterwards, the reference control system for the comparison and the evaluation method for the analysis are described. In section Class-based control concept the investigated control system with the ASI and simulation results under ideal conditions are explained. Main part in section 4 contains the comprehensive robustness analysis and evaluation of the control system. Finally, a summary is given.

2. Simulation setup

For the evaluation of the control concept with ASI, spatial and temporal resolved DNI maps are used in the simulation tool VSF. It is compared to a reference controller, which has only DNI information from a few measuring points.

2.1. Camera systems used to provide DNI maps

Spatial DNI information with a sufficient temporal and spatial resolution for CSP control applications can be derived from camera based nowcasting systems. Two distinct general approaches are conceivable. Firstly, the ASI, which consist of upward facing cameras with fisheye lenses used to detect clouds in the sky (Hasenbalg et al. 2020) and a raytracing algorithm projects the shadows on the ground. Secondly, downward facing cameras mounted on the top of a high building (Kuhn et al. 2017) or on the top of a mountain range (Wilbert et al. 2020). These so-called shadow cameras take images of the ground, in order to detect actual cloud shadows and are thus more accurate.

Both approaches are used in this work. An ASI system provides DNI information for the solar field controllers, whereas the shadow camera system provides the real spatial DNI conditions acting on the simulated solar field in section 4.1. Both systems were operated in parallel at CIEMAT's Plataforma Solar de Almería (PSA).

From the available DNI measurement data, a number of 28 days for the measurement system ASI and 23 days for the measurement system shadow cameras were selected. All the shadow camera days are included in the 28 ASI days, so a set of 23 days is available with two different DNI sources. DNI levels and variability of these days are illustrated in Fig. 1 for the ASI system and in Fig. 2 for the shadow camera system. The plotted DNI is the mean value over all collectors of the solar field. It is plotted over the time of the day in UTC + 0. Below a mean DNI value of 130 W/m^2, the color bar changes to blue in order to indicate the threshold for the ability to reach the nominal outlet temperature of 393 °C with the minimum allowed mass flow in the solar field. The time interval covered by the DNI maps on each day is limited to the interval where the sun elevation angle is above 12°, calculated with the Michalsky sun algorithm (Michalsky 1988). These days have been chosen in a way such that a broad variety of different irradiation conditions

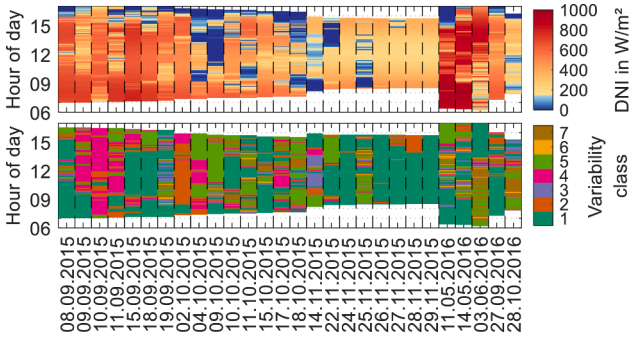

Fig. 1. DNI values form ASI system.

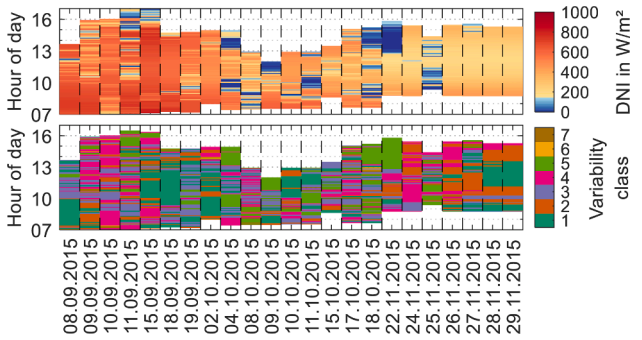

Fig. 2. DNI values from shadow camera system.

is covered. Some days (given in DD.MM.YYYY format) have periods with rather low DNI (09.10.2015, 14.11.2015 and 25.11.2015), whereas other days have high irradiance up to clear sky conditions (15.09.2015, 15.10.2015 and 14.05.2016).

The plotted variability classes, described in section 3, indicate that cloud situation may change many times over the day. For example, on the 04.10.2015 the day starts with class 2 “clouds with high transmittance”, continuing with class 4 “many clouds without quick changes”, alternating with class 5 “complete overcast of the solar field”. Different measurement periods between both camera systems, such as on 09.10.2015, are considered by simulating only the times in which DNI maps from both systems are available. A comparison of the systems and the generated DNI maps is described in Nouri et al. (2018).

2.2. Virtual solar field simulation model

Commercial PT power plants require a large area to collect enough solar energy. For example, the whole La Africana solar power plant covers an area of about 2.52 km^2 (NREL 2020b). Due to the large stretch, partial shading of the collector loops can take place, making it necessary to simulate all loops in the field to get realistic estimations of the energy yield. Simulation tools can provide a virtual testing platform that is valuable for the development of control systems by modeling the thermal behavior of such a large solar field.

The simulation tool VSF used in this paper was developed at the Institute of Solar Research at German Aerospace Center (Noureldin 2018). It models the individual pipes starting after the power block with the cold header, to the subfields and individual loops and via the hot header back to the power block. By implementing different collector types, receivers and HTFs, a flexible deployment is guaranteed. Hydraulic and thermal calculation is performed for each individual pipe and collector in the solar field, which allows simulating different irradiation situations with spatially resolved DNI maps.

2.3. Applied state of the art solar field control

For comparison of the innovative control concepts, a reference control system is used that represents a control scheme found in a similar form in many plants today. The same simulations are carried out with the reference controller and evaluated based on the most important criteria.

The control system includes mainly two control loops, namely the local SCA temperature controllers and the total field mass flow controller. A detailed description of the control concept used is presented in Noureldin et al. (2017) and Noureldin et al. (2021). For comparison with the innovative control schemes, the most important elements of the reference control concept are summarized in the following paragraphs.

Each local SCA controls the HTF temperature, which is measured in the center of each SCA. The manipulated variable that is changed by the feedback (FB) proportional integral (PI) controller is the tracking angle of the SCA relative to the theoretical tracking angle derived from the sun position. Temperature setpoints are calculated individually for each of the four SCAs in the loop based on the loop inlet temperature and the design field outlet temperature. As an additional protection, a maximum temperature limitation is determined, at which the SCA moves completely out of focus to prevent damage to the components or degradation of the HTF due to overheating. This scenario is referred to as emergency defocusing.

The second control loop assures that the design field outlet temperature is reached by adapting the HTF mass flow according to the current irradiation level and outlet temperature. Fig. 3 shows the structure of this controller. A FF controller calculates a theoretically required mass flow using the thermal input from the DNI, the thermal losses and the average heat capacity of the HTF inventory. Since the FF calculation suffers from inaccuracies in the measured DNI level and from inconsideration of transient behaviors, an additional FB control loop is introduced.

The temperature PI controller uses the average measured loop outlet temperature to calculate an adjustment of the mass flow rate from the FF part. An adaptive calculation of the parameters based on the first-order plus deadtime method is performed in each time step based on the thermal state of the solar field. Last part of the control concept is a focus PI controller, which ensures that the focus rate is kept at a high level, ideally at 100%. If the average focus rate tends to decrease, the mass flow is increased and vice versa. Based on these three control elements, a mass flow set point is generated. The pump PI controller controls the pump differential pressure so that the required mass flow rate is achieved. All parameters for the controllers for the used field configuration are listed in Table 1. In this and the following tables, a qualitative description is used for the factor f_C. Here, “conservative” describes the value of 5, “moderate” of 1, “aggressive” of 0.5 and “very aggressive” of 0.1.

2.4. Evaluation methodology

VSF can be utilized to compare different control systems by computing the profiles of temperature, mass flow, etc. over the simulation period. This data is post-processed in order to condense the information according key performance indicators that can be used to compare different concepts. A number of criteria are used in this study. For the technical evaluation, the RMSE of the solar field outlet temperature, focus rate and emergency defocusing are considered. For the evaluation, the data is used in which the average DNI is above the minimum in which the set outlet temperature can be reached. In addition, only the periods when the control system is active are evaluated. This means that start-up and recirculation are not included in this evaluation. As a final result, the reduction of the RMSE of the outlet temperature and the increase of the solar field focus compared to the reference controller is presented. For emergency defocusing the number of events is summed up and compared to the absolute number observed for the reference control strategy.

For the economic evaluation, the electrical yield of the respective day is calculated from the simulated results. Following is only a brief summary of the approach. The detailed approach is described in Noureldin (2018) and Noureldin et al. (2021). Electrical yield under transient cloud conditions is lower than the ideal electrical yield. An impact of transient behavior is represented by penalties. The first penalty considers the electrical yield losses due to the defocusing of the collectors and thus the thermal energy which is not collected. The second penalty takes into consideration the outlet temperature of the solar field. A reduced outlet temperature influences the power block efficiency and thus the electrical yield. At the same time, a reduced outlet temperature has an impact on the utilization of the thermal storage. A specific penalty has been developed that generates a reduction of produced energy by not fully utilizing the storage capacity in periods where the storage is completely charged. By means of these three penalties, the losses of the

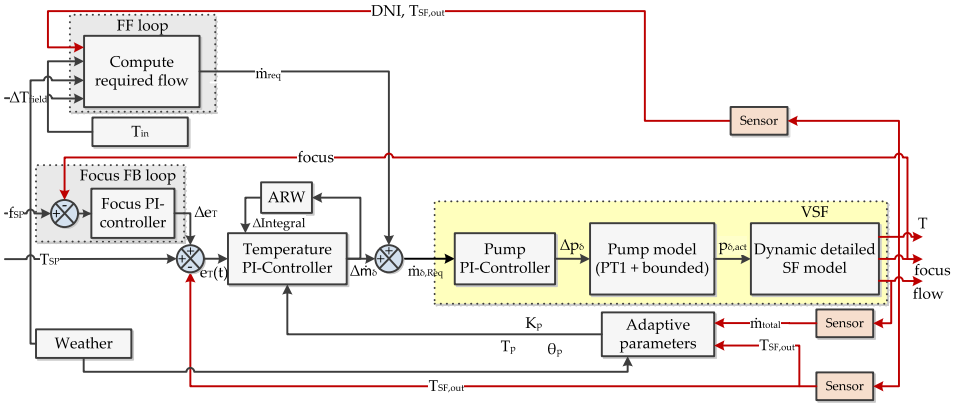

Fig. 3. The control diagram for the mass flow controller in the power block for calculating the mass flow for the solar field (Müllner 2020).

Table 1
Control parameters for the reference controller.

Parameter	temperature FB controller ($\dot{m}$)	focus feedback controller ($\dot{m}$)	temperature FB controller (SCA)
Process gain, K_p	adaptive	$3\%/^{\circ}C$	$-6\ ^{\circ}C/deg$
Process time constant, T_p	adaptive	160 s	115 s
Process deadtime, θ_p	adaptive	adaptive	adaptive
Controller behavior, f_C	aggressive	aggressive	moderate

simulated days are determined and subtracted from the theoretical maximum achievable electrical yield.

3. Class-based control concept

This section describes and evaluates the advanced control concept using DNI maps created for the current situation. This concept makes use of an improved feed-forward element for the mass flow estimation based on improved DNI values from the ASI system and an extended concept for adaptive parameters based on the cloud situation derived from the ASI system.

This so-called class-based control concept requires a classification of the cloud situation, which is composed of a spatial and temporal classification of the DNI situation provided by the ASI system. For each identified class, an individual factor for the focus and temperature PI-controller of the mass flow controller is defined. DNI maps of the ASI system can be classified into eight temporal classes (Schroedter-Homscheidt et al. 2018) and five spatial classes (Schlichting 2018). These defined classes are used to change the control behavior depending on the weather condition in the solar field. In order to reduce the number of possible combinations of temporal and spatial classes, class combinations with similar effects on the controller setting are combined (Schlichting 2018). These seven resulting combined classes are shown in Table 2.

Table 2
Combination of temporal and spatial variability classes used for the adaptation of controller settings.

Combined class	Spatial class	Temporal class	General description
1	1	no condition	Clear sky
2	2	no condition	Clouds with high transmittance
3	3	1–3, 5–8	Partly cloudy, no small quick clouds
4	4	1–3, 5, 7, 8	Many clouds, no quick clouds
5	5	no condition	Overcast with low transmittance
6	3	4	Partly cloudy with some quick clouds
7	4	4, 6	Many and quick clouds

Class dependent modification of controller settings is realized by introducing a factor as already defined in section 2.3. Simulations have been performed with all combinations of different factors in order to find those factors best suited for the respective DNI conditions of the variability class (Schlichting 2018). From this analysis two setups of assignments have been derived. The setup called objective temperature performed very well in keeping the outlet temperature at the design value, whereas the setup called objective focus rate reached a better overall focusing at the cost of reduced average temperature. Since both objectives might be relevant for future applications both setups have been used to generate the final results. The factor assignments are given in Table 3 and Table 4, respectively.

3.1. Simulation results under ideal conditions

An ideal set of conditions is used to test the reference control concept and the two class-based control concepts. Ideal conditions comprise a perfectly working ASI system (ASI generated DNI maps are exactly the DNI situation on the field), a perfect match between the real solar field performance and the energy balance model used in the feed forward controller (e.g. no soiling), and a constant solar field inlet temperature of 290 °C. The aim of these simulations is to verify the functionality of the controllers and to show the theoretical potential of control concepts making use of an ASI system. A robustness analysis is carried out in section 4 to evaluate the performance under non-ideal conditions.

Simulation results are provided in Table 5. It can be observed that the class-based controllers achieve a higher electrical yield by about 2.7% than the reference controller. In addition to the electrical yield criterion, other technical performance indicators are relevant. On the one hand, the controller with the objective temperature can reach the electrical yield by reducing the RMSE of the outlet temperature by 9.58% and a 0.95% higher focus rate. In addition, the amount of emergency

Table 3
Controller parameters for the controller setup “objective temperature”.

Parameter	Combined class	temperature FB controller ($\dot{m}$)	focus FB controller ($\dot{m}$)	temperature FB controller (SCA)
K_p	1–7	Adaptive	$3\%/^{\circ}C$	$-2\ ^{\circ}C/deg$
T_p	1–7	Adaptive	160 s	50 s
θ_p	1–7	Adaptive	adaptive	adaptive
f_C	1	Moderate	very aggressive	moderate
	2	Aggressive	aggressive	moderate
	3, 4	Moderate	deactivated	moderate
	5–7	Aggressive	deactivated	moderate

Table 4
Controller parameters for the controller setup "objective focus rate".

Parameter	Combined class	temperature FB controller ($\dot{m}$)	focus feedback controller ($\dot{m}$)	temperature FB controller (SCA)
K_p	1–7	Adaptive	$3\%/^{\circ}C$	$-6\ ^{\circ}C/deg$
T_p	1–7	Adaptive	160 s	115 s
θ_p	1–7	Adaptive	adaptive	adaptive
f_C	1	Moderate	very aggressive	moderate
	2	Aggressive	aggressive	moderate
	3	Conservative	deactivated	moderate
	4	Moderate	moderate	moderate
	5	Conservative	moderate	moderate
	6	Aggressive	deactivated	moderate
	7	Aggressive	deactivated	moderate

defocusses can be decreased by 42.68%. On the other hand, the controller with the objective focus rate can improve the focus rate by 1.41%, the RMSE of the outlet temperature by 8.19% and decreases the amount of emergency defocuses by 27.69%. Overall, it can be concluded that the class-based controllers can improve the result in every technical aspect.

4. Robustness analysis of the class-based control concept

In section 3.1, the class-based control concept was evaluated under ideal conditions. In a real application, uncertainties occur in the system and it is important that the control system reacts robustly. In order to analyze the robustness, different scenarios are simulated with the simulation tool VSF. In the simulations, only the current values of the ASI are used. Available forecasts for up to 20 min (as available from the ASI system) do not result in additional performance improvements. More detailed research on the DNI forecasts in the control system is described in Noureldin (2018), Müllner (2020) and Kotzab et al. (2020).

4.1. Quality of the ASI irradiation measurement system

DNI maps generated by the ASI system suffer from uncertainties in the measurement and processing (Nouri et al. 2018). For the investigation on how these uncertainties impact the control system, a second, independently derived, set of spatial-temporal irradiance data is used. These DNI maps are generated by the shadow camera system as introduced in section 2.1. The shadow camera DNI maps are used for the VSF simulation (representing the real conditions on the field) and the ASI derived DNI maps are used as the estimates of the real irradiance situation available to the control system. A first investigation of such setup is described in (Nouri et al. 2020). The authors introduced an extended class-based control concept called hybridized control. An estimate of the expected current uncertainty level is available as an additional information from the ASI system. Depending on the expected accuracy of the ASI derived DNI maps, either the class-based controller setup or the reference controller setup is used. The class-based control concept and thus the information from the ASI system is used in situations where low uncertainty of the ASI derived DNI values is expected. In all other situations, the reference controller is applied.

For consistent result data, the approaches of Nouri et al. (2020) are carried out with the current simulation setup. Daily results in terms of yield are shown in Fig. 4. On most days, the concept shows an improvement compared to the reference control. The electrical yield can be increased by 1.41% compared to a value of 2.7% obtained for ideal irradiation conditions. On the technical side, the RMSE of the solar field outlet temperature can be reduced by 9% and the emergency defocusing by 48%. The average focusing in the solar field can be increased by 0.6%. The results show that the developed control concept still operates robustly and generates benefits compared to the reference control. Nevertheless, the uncertainty in irradiation values reduces the benefits in all categories. Furthermore, Fig. 4 shows an improvement in performance in different situations. In this way, the electrical yield can be increased with the class-based control concept on days with good DNI and clear sky, such as 08.09.2015, or with good DNI and very variable conditions, such as 10.09.2015. On the other hand, the electrical yield can also be increased on autumn days with low DNI and different irradiation conditions, such as 26.11.2015 and 29.11.2015.

4.2. Variable solar field inlet temperature

The control development as described in the previous section assumes a constant solar field inlet temperature of 290 °C as it is typical for today parabolic trough plants. Under part load conditions, the oil coming back from storage or steam generation will have lower temperature so the control concept needs to be checked for robustness under varying inlet temperatures. The investigation of different inlet temperatures is carried out in two steps. In the first step simulations are carried out with constant solar field inlet temperatures in the range of 270 °C to 310 °C. By this study, the general suitability of the control concept at various constant inlet temperature levels can be shown. In a second step, the inlet temperature is modified in a sine-shaped way to represent dynamic changes during operation. The temperature changes in a period of 25 min by 10 °C. The frequency of the sine curve is chosen to represent expected transients in field inlet temperature. Due to large

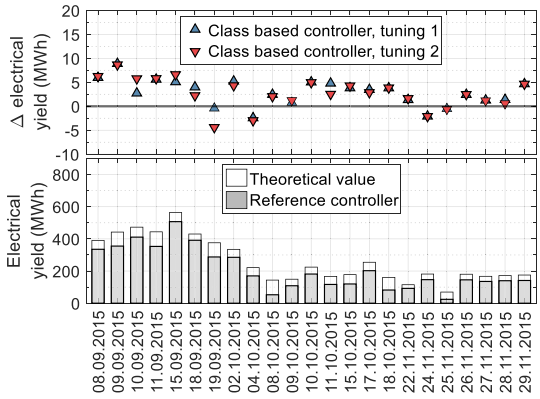

Fig. 4. Evaluation of the class-based control concept with uncertain irradiation conditions for 25 days. Tuning 1 is class-based controller variant "objective temperature" and tuning 2 "objective focus rate".

Table 5
Performance of the two class-based controller variants "objective temperature" and "objective focus rate" under ideal conditions. Values represent averages over the 28 example days. Percentage values indicate difference to reference controller.

Controller setup	Total electrical yield (increase in %)	RMSE HTF temperature (decrease in %)	Focus rate (increase in %)	Total emergency defocusses (decrease in %)
"Reference"	267.30 MWh	7.60 °C	97.09%	19,853
"Objective temperature"	274.57 MWh (+2.72%)	6.88 °C (−9.58%)	98.02% (+0.95%)	11,380 (−42.68%)
"Objective focus rate"	274.42 MWh (+2.67%)	6.98 °C (−8.19%)	98.46% (+1.41%)	14,356 (−27.69%)

thermal inertia of inlet piping, no very steep temperature gradients are to be expected.

Table 6 gives the results of the simulations with constant inlet temperature levels. Base line are the values at 290 °C from the previous investigations. For lower or higher inlet temperatures, the performance values slightly differ but are still close to the baseline. The normalized increase of the outlet temperature describes the average increase of the HTF temperature depending on the inlet temperature. Through normalization, a comparison of the respective inlet temperatures can be made to identify the behavior. The calculation is carried out as follows:

$$T_{norm} = \frac{T_{out,setpoint} - T_{out}}{T_{out,setpoint} - T_{in}} \quad (1)$$

The increase of the outlet temperature and focusing of the collectors is almost constant at all inlet temperatures, which means a robust behavior of the controller at the different situations. In case of emergency defocusing, an increase can be seen as the inlet temperature is increased. An increase in emergency defocusing can be explained by the increased required mass flow as the temperature difference between inlet and outlet of the loops is lower. Due to the limitation of the pump power, the number of emergency defocusing increases when the irradiation is too high.

When the inlet temperature is dynamically changed in a sine-shape form, the results shown in Fig. 5 still show an improvement compared to the reference controller. In total, the electrical yield can be increased by 3.4% (base line 2.7%). In the technical evaluation, a 30% reduction in RMSE of the outlet temperature (base line 9%), a 1.5% increase in focus rate (base line 1.2%) and a 50% reduction in emergency defocus (base line 35%) are possible. The results show that the varying inlet temperature does not significantly impact the controller performance even a slightly better performance is observed under the dynamic boundary conditions.

4.3. Sample time of the control system

In the above presented studies, a 30 s sampling time was considered for the controller. This means, that the controller provides a new value every 30 s. This sampling time was chosen since it represents a standard update interval of the ASI system. Apart from the ASI update cycle the sampling time also covers time lags in the digital control system data processing. The impact of sampling time on the controller performance is studied for sampling times between 2 and 60 s. Results listed in Table 7 indicate no significant changes in the areas of revenue, outlet temperature and focus. In case of emergency defocus, an increase can be detected with higher sample times.

The analysis demonstrates that higher sample times can lead to a higher number of emergency defocuses. The update time of the sensor data in the solar field and the calculation of the DNI maps from the ASI system should ensure that the sample time of the control system is as short as possible.

Table 6
Simulation results with different but constant solar field inlet temperatures using controller setup "objective temperature". Difference to the base line 290 °C are given in brackets.

Solar field inlet temperature	Normalized temperature increase	Focus rate (Increase in %)	Emergency defocus (Decrease in %)
270 °C	0.77	98.43% (0.42%)	11,385 (0.04%)
280 °C	0.77	98.44% (0.43%)	10,961 (−3.68%)
290 °C	**0.78**	**98.02%**	**11,380**
300 °C	0.80	97.96% (−0.06%)	15,002 (+31.82%)
310 °C	0.80	97.47% (−0.56%)	17,644 (+55.04%)

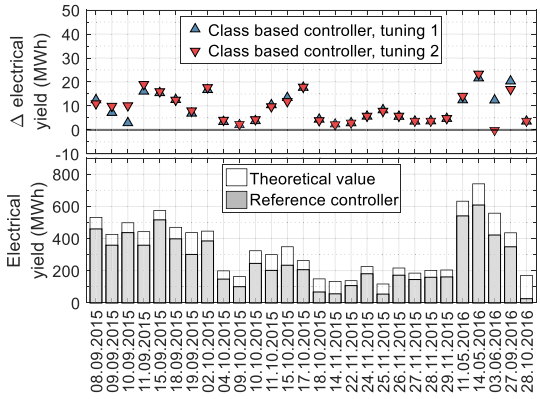

Fig. 5. Performance of the class-based controller against the "reference controller" under dynamically changed solar field inlet temperatures.

Table 7
Performance of the class-based controller "objective temperature" with different sampling times. Relative differences to the base line of 30 s are given in brackets.

Sample Time controller	Total electrical yield (increase in %)	RMSE HTF temperature (decrease in %)	Focus rate (increase in %)	Total emergency defocusses (decrease in %)
2 s	274.41 MWh (−0.06%)	7.04 °C (1.88%)	98.07% (0.05%)	11,020 (−3.16%)
10 s	274.42 MWh (−0.06%)	7.02 °C (1.60%)	98.05% (0.04%)	10,923 (−4.02%)
20 s	274,46 MWh (−0.04%)	6.99 °C (1.16%)	98.04% (0.02%)	11,095 (−2.50%)
30 s	**274.57 MWh**	**6.91 °C**	**98.02%**	**11,380**
40 s	274.78 MWh (+0.07%)	6.81 °C (−1.54%)	97.97% (−0.05%)	11,708 (2.88%)
50 s	275.18 MWh (+0.22%)	6.73 °C (−2.61%)	97.74% (−0.28%)	15,092 (32.62%)
60 s	274.90 MWh (+0.12%)	6.61 °C (−4.44%)	97.88% (−0.14%)	13,717 (20.54%)

4.4. Soiling in solar field

The control system was developed under the assumption of clean mirrors considering 0% soiling. If soiling occurs the used energy balance in the FF loop does not exactly represent the situation in the field. Thus, the estimated mass flow deviates from the required flow in the real field. In order to check the controller performance under these conditions, scenarios with different homogeneous soiling of 5% (Case 1) and 10% (Case 2) over the four subfields are simulated. Since the soiling evolution over time is not considered in this investigation, the soiling values are kept at the same value for all simulated days. Thus, in the scenario 5% homogeneous soiling scenario, a cleanliness of 95% is guaranteed for each SCA over the complete simulation.

Due to equal mass flows in the different loops, there are significant effects on the temperature distribution in the loops occur in case of soiling is not equally distributed over the field. For this case, the control behavior is simulated assuming an inhomogeneous soiling among the subfields (Case 3). One single soiling value is used for all collectors in each of the four subfields (subfield 1: 0%, subfield 2: 3.3%, subfield 3: 6.6% and subfield 4: 10%).

Table 8 lists the results under these scenarios. These are the results of the class-based controller objective temperature for each case. Although the FF part of the controller does not have knowledge of the real soiling values (but assumes a value of 0%), a robust behavior of the control system can be generally identified. With a homogeneous soiling of 5% an

Table 8
Simulations results of the class-based controller "objective temperature" with different soiling situations. Controller assumes a soiling rate of 0% whereas the real field shows homogeneous fixed soiling values of 0%, 5%, 10% and an inhomogeneous fixed soling value, respectively.

Solar field soiling	RMSE HTF temperature (decrease in %)	Focus rate (increase in %)	Total emergency defocusses (decrease in %)
homogenous 0%	**6.91 °C**	**98.02%**	**11,380**
(Case 1) homogenous 5%	7.70 °C (11.38%)	97.55% (−0.47%)	13,101 (15.12%)
(Case 2) homogenous 10%	8.62 °C (24.70%)	98.01% (−0.01%)	10,224 (−10.16%)
(Case 3) Inhomogeneous 0%, 3.3%, 6.6%, 10%	7.64 °C (10.50%)	97.75% (−0.27%)	11,076 (−2.67%)

increase in emergency defocusing can be seen. The theoretical calculation of the mass flow in the FF with assuming of 0% fixed soiling values results in a too high mass flow, which must be compensated by the PI controllers. If the factor used to calculate the control parameters is too low (higher aggressivity of the controller), the total mass flow for the solar field may become too low, which means a higher number of emergency defocusing. In this case the parameter should be adjusted to decrease the number of emergency defocusing. If the soiling is even higher (10%), the selected factor for calculating the mass flow is not very aggressive, since the mass flow would have to be further adjusted to the conditions in order to achieve a better solar field outlet temperature.

If the controller knows about the soiling values in the field, the performance in terms of outlet temperature stability improves. This is true even at high soiling rates of 10%. Table 9 provides the results for the same setups as in Table 8 with the soiling information passed over to the control system. It is also observed that the controller can achieve good performance under inhomogeneous soiling conditions also when it is given only an average value. This means that the control system in the inhomogeneous soiling scenario uses an average value of 5% of fixed soiling values to calculate the mass flow for the solar field. Despite the increase in emergency defocusing events, very slight effect is observed on the total collected energy as seen by the focus rates. The results suggest that condition monitoring systems could help in improving the RMSE of the outlet temperature by providing good estimates of the real soiling situation.

The results shown so far are based on equal soiling values within at least a subfield. In a next step, an inhomogeneous distribution within the subfield itself is defined as more realistic test case. A simulator was created by Horstmann (2021) that calculates an individual soiling value for each loop of the field assuming an homogeneous soiling rate of 0.5% per day with a standard deviation of 0.2%. This reflects typical soiling conditions at PSA. The simulator furthermore assumes that three loops can be cleaned per day. From the soiling rate and the cleaning actions, it determines soiling distributions across the loops. Fig. 6 shows an example for the distribution of fixed soiling values over the field, which are used for the simulations (Case 4).

Table 9
Simulations results of the class-based controller "objective temperature" with different soiling situations. The solar field shows homogeneous fixed soiling values of 0%, 5%, 10% and an inhomogeneous fixed soling value. The controller knows the fixed soiling values and uses them in the calculation.

Solar field soiling	RMSE HTF temperature (decrease in %)	Focus rate (increase in %)	Total emergency defocusses (decrease in %)
homogenous 0%	**6.91 °C**	**98.02%**	**11,380**
(Case 1) homogenous 5%	7.34 °C (6.13%)	97.61% (−0.42%)	13,190 (15.90%)
(Case 2) homogenous 10%	7.53 °C (8.86%)	97.71% (−0.31%)	12,640 (11.07%)
(Case 3) Inhomogeneous 0%, 3.3%, 6.6%, 10%	7.40 °C (7.08%)	97.74% (−0.28%)	13,570 (19.25%)

Simulation results are shown in Fig. 7. The electrical yield can be increased by 3.1% in total for all the investigated simulations. Technically, the RMSE of solar field outlet temperature can be decreased by 8% and the focus of solar field increased by 0.4%. A reduction of 27.1% in emergency defocus can be achieved.

4.5. Combination of the different situations

In this study, the individual scenarios on non-ideal situations described in the above sections are combined. For this setup, the control system assumes a fixed soiling value of 0% whereas the real field has the inhomogeneous soiling distribution shown in Fig. 6 (Case 4). The solar field inlet temperature follows the variation described in Section 4.2. Finally, the controller used the DNI information from the ASI system whereas the field sees the DNI generated from the shadow camera system. The daily evaluation of the electrical yield is shown in Fig. 8. The individual days show similar improvements in electrical yield as in the individual robustness analyzes. The electrical yield can be increased by 2% over all days. Technically, a 6% reduction of RMSE of the outlet temperature, a 1.5% increase in focus and a 48% reduction in emergency defocus can be achieved. In general, a robust behavior of the control concept can be proven with the combination of the scenarios.

The combination of the individual effects shows on the one hand that the class-based regulation concept reacts robustly and on the other hand that there is an improvement in all the investigated criteria. These results are the basis for an economic evaluation based on an annual yield simulation with the software Greenius (Dersch and Dieckmann 2021) assuming a selling price of 192 € for each MWh. Thus, an increase in revenue can be achieved due to the improved controller performance on the investigated days. On days with good irradiation (08.09.2015, 15.09.2015 and 18.09.2015), the revenue could be increased by 2.78% on average. This corresponds to an additional revenue of 6101.66 € on these three days. On days with worse irradiation conditions including many clouds or low DNI (09.10.2015, 25.11.2015 and 28.11.2015), the revenue can be increased by 1.19%, which corresponds to 1077.87 €.

4.6. Using the controller on a solar field with different layout

The developed control concept can be parametrized for other configurations by just a few parameters. This enables the controller to be easily transferred to a new solar field configuration. The Andasol-3 (NREL 2020a) power plant configuration in Spain is used as a test case. Same ideal conditions as in section 3.1 are simulated. In order to

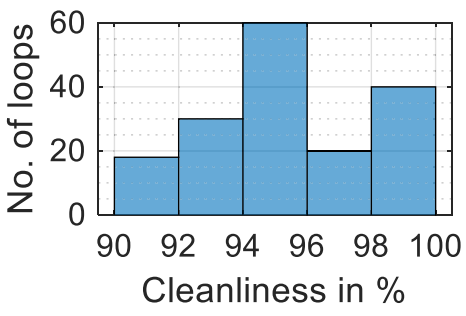

Fig. 6. Cleanliness of the solar field for the simulation setup.

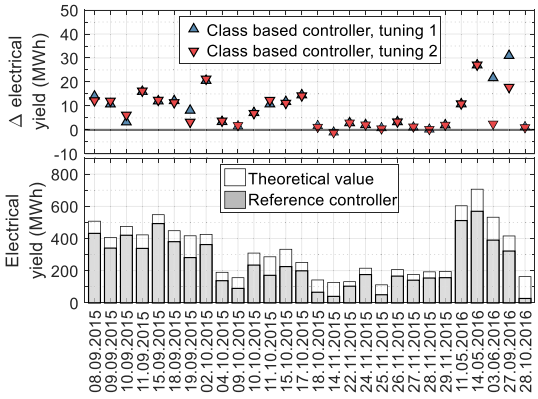

Fig. 7. Performance of the class-based controller against the "reference controller" under inhomogeneous soiling of the solar field.

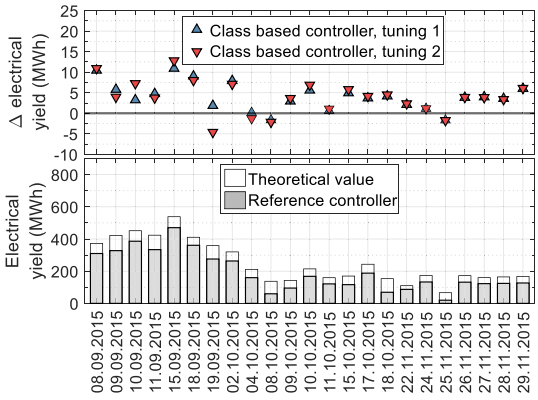

Fig. 8. Performance of the class-based controller assuming non-ideal conditions in soiling, DNI values, and solar field inlet temperature.

use the same test days, the plant location is assumed to be Tabernas (PSA) instead of the real Andasol-3 site. Whereas the La Africana plant is equipped with two pyrheliometer stations, Andasol-3 uses five stations. The result of the simulation is presented in Fig. 9. The evaluation of the electrical yield shows an improvement with the new control concept on almost all days. Overall, an increase in electrical yield of about 1.54% can be achieved. Compared to the results of 2.7% obtained for the La Africana layout the performance increase is smaller. This is attributed to the effect of the better performance of the reference control, since the reference controller uses the pyrheliometer station values to estimate the mass flow in the feed forward control loop. Thus, the five stations

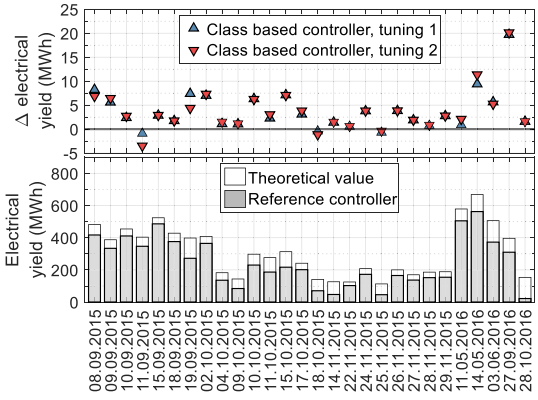

Fig. 9. Daily electrical yield of the robustness analysis with a different power plant solar field (Andasol-3).

reflect a more accurate average DNI value than the setup with only two stations.

The technical evaluation results show improvements in the RMSE of the solar field outlet temperature of 6%, in focus rate of 0.8% and in emergency defocusing of 55%. By a simple switch of the geometry and adaptation of a couple of parameters, it is demonstrated that the control system can easily be transferred to a new layout.

5. Conclusion

PT plants are state of the art technology using established control logics for the solar field. Under varying irradiation conditions like clouds passing over the field, it is a systematic challenge to maintain the design outlet temperature and to operate with all collectors in full focus. The reasons behind are control actions induced by a local misbalance of irradiation received on the collectors and the heat transfer fluid flow in the receiver tube of the respective section. This is, in particular, the case for configurations which do not employ individually controlled valves at the inlet of each loop.

The objective of the presented work is to show that the control behavior of a PT field can be improved by utilizing spatially and temporarily resolved irradiance data originating from an ASI system. Whereas the principles of the control concept have already been published in earlier work, the focus of this paper is on a robustness analysis that proves that the approach is applicable also under non-ideal conditions. Simulation studies with a detailed solar field model called VSF have been conducted under different scenarios chosen to represent non-ideal situations as they would occur in a real field. This investigation was possible since spatio-temporal irradiance data from two different sources, namely the ASI system and a shadow camera system, was available for many days.

DNI information obtained from the ASI system is used by the control system to, firstly, calculate the theoretically required mass flow by means of a field efficiency model and, secondly, to estimate the controller parameters adaptively. The new control approach is compared to a benchmark control concept based on a few DNI stations in the field without access to spatially resolved DNI from the ASI system. The manipulated variables are the mass flow into the field and the tracking position of each collector to control the fluid temperatures. It is shown that the use of the current and preceding ASI images is sufficient for the control purpose.

For the robustness analysis, realistic scenarios that compromise non-ideal conditions were chosen for the simulations. Individual scenarios cover the effect of uncertainties in the DNI maps originating from the ASI system, of lower solar collection efficiencies induced by, for example, soiling, of variations in solar field inlet temperature originating from storage or steam generator, as well as of non-continuous update cycles of the control system. In a first step, the above effects were analyzed individually before being combined in one single simulation. For the evaluation, a number of 23 representative days were selected covering different irradiation situations.

The results clearly show that the control concept operates robustly under the various scenarios. Under all conditions, the ASI based control system is able to improve the performance compared to the benchmark case. In the combined uncertainty scenario, the ASI control concept is able to increase the electrical yield by 2%. On the technical side, a 6% reduction in RMSE of the outlet temperature, a 1.5% increase in focus rate and a 48% reduction in emergency defocusing events are observed. In addition, the economic analysis showed that the revenue can be increased on days with good conditions (2.78%) as well as on days with poor DNI conditions (1.19%).

Finally, the transfer of the control concept to another solar field configuration was tested. Since the control concept requires only a few descriptive parameters of the solar field configuration, adapting of the control concept from the original La Africana field configuration to the Andasol-3 field configuration is a simple procedure.

The comprehensive simulation studies carried out with the detailed transient field simulation tool VSF under realistic conditions demonstrate that the ASI based control concept improves the annual financial revenues of the investigated parabolic trough fields by about 2%. Due to the low investment costs for the installation of an ASI system, it can be considered an efficient way to improve the plant economy even for existing systems. This thorough evaluation especially considering realistic conditions provides the scientific basis for first demonstration in a commercial-scale plant.

Declaration of Competing Interest

The authors declare that they have no known competing financial interests or personal relationships that could have appeared to influence the work reported in this paper.

Acknowledgement

Funding was received by the German Federal Ministry for Economic Affairs and Energy within the WobaS-A project (Grant Agreement 0324307A).

Thanks to the colleagues from the Solar Concentrating Systems Unit of CIEMAT for the support provided in the installation and maintenance of the shadow cameras. These instruments are installed on CIEMAT's CESA-I tower of the Plataforma Solar de Almería.

References

Barcia, L., Peón Menéndez, R., Martínez Esteban, J., José Prieto, M., Martín Ramos, J., de Cos Juez, F., Nevado Reviriego, A., 2015. Dynamic Modeling of the Solar Field in Parabolic Trough Solar Power Plants. Energies 8 (12), 13361–13377.

Camacho, E.F., Rubio, F.R., Berenguel, M., Valenzuela, L., 2007a. A survey on control schemes for distributed solar collector fields. Part I: Modeling and basic control approaches. Sol. Energy 81 (10), 1240–1251.

Camacho, E.F., Rubio, F.R., Berenguel, M., Valenzuela, L., 2007b. A survey on control schemes for distributed solar collector fields. Part II: Advanced control approaches. Sol. Energy 81 (10), 1252–1272.

Cole, W., Frazier, A.W., 2020. Cost Projections for Utility-Scale Battery Storage: 2020 Update. N. R. E. Laboratory, Golden CO.

Dersch, J., Dieckmann, S., 2021. greenius - The Green Energy System Analysis Tool.

Hasenbalg, M., Kuhn, P., Wilbert, S., Nouri, B., Kazantzidis, A., 2020. Benchmarking of six cloud segmentation algorithms for ground-based all-sky imagers. Sol. Energy 201, 596–614.

Horstmann, S., 2021. Online Optimization - Cleaning strategies for CSP plants.

IRENA, 2021. Renewable capacity statistics 2021. International Renewable Energy Agency (IRENA), Abu Dhabi.

Kotzab, T., Hirsch, T., Nouri, B., Yasser, Z., Angulo Duque, D., 2020. Using DNI Forecasts provided by All Sky Imager to improve Control of Parabolic Trough Solar Fields. SolarPACES 2020. Online.

Kuhn, P., Wilbert, S., Prahl, C., Schüler, D., Haase, T., Hirsch, T., Wittmann, M., Ramirez, L., Zarzalejo, L., Meyer, A., Vuilleumier, L., Blanc, P., Pitz-Paal, R., 2017. Shadow camera system for the generation of solar irradiance maps. Sol. Energy 157, 157–170.

Michalsky, J., 1988. The Astronomical Almanac's algorithm for approximate solar position (1950–2050). Sol. Energy 40, 227–235.

Müllner, S., 2020. Situationsangepasste Reglerparametrierung für Parabolrinnenkraftwerke.

Noureldin, K., 2018. Modelling and Control of Transients in Parabolic Trough Power Plants with Single-Phase Heat Transfer Fluids. Doktors der Ingenieurwissenschaften Rheinisch-Westfälischen Technischen Hochschule Aachen.

Noureldin, K., Hirsch, T., Kuhn, P., Nouri, B., Yasser, Z., Pitz-Paal, R., 2017. Modelling an Automatic Controller for Parabolic Trough Solar Fields under Realistic Weather Conditions.

Noureldin, K., Hirsch, T., Nouri, B., Yasser, Z., Pitz-Paal, R., 2021. Evaluating the Potential Benefit of Using Nowcasting Systems to Improve the Yield of Parabolic Trough Power Plants with Single-Phase HTF. Energies 2021 (14), 773.

Nouri, B., Kuhn, P., Wilbert, S., Prahl, C., Pitz-Paal, R., Blanc, P., Schmidt, T., Yasser, Z., Ramirez, L., Heinemann, D., 2018. Nowcasting of DNI Maps for the Solar Field Based on Voxel Carving and Individual 3D Cloud Objects from All Sky Images. SolarPACES Conference. Santiago de Chile.

Nouri, B., Noureldin, K., Schlichting, T., Wilbert, S., Hirsch, T., Schroedter-Homscheidt, M., Kuhn, P., Kazantzidis, A., Zarzalejo, L.F., Blanc, P., Yasser, Z., Fernández, J., Pitz-Paal, R., 2020. Optimization of parabolic trough power plant operations in variable irradiance conditions using all sky imagers. Sol. Energy 198, 434–453.

NREL, 2020a. Andasol-3 | Concentrating Solar Power Projects. Retrieved 22.07.2020, 2020, from https://solarpaces.nrel.gov/andasol-3.

NREL, 2020b. La Africana | Concentrating Solar Power Projects. Retrieved 16.06.2020, 2020, from https://solarpaces.nrel.gov/la-africana.

Schlichting, T., 2018. Bewertung der Verwendbarkeit von Strahlungskarten für den Einsatz in der Regelung eines Parabolrinnensystems. Universität Duisburg-Essen, Master Mechatronik.

Schöniger, F., Thonig, R., Resch, G., Lilliestam, J., 2021. Making the sun shine at night: comparing the cost of dispatchable concentrating solar power and photovoltaics with storage. Energy Sources, Part B: Econ., Plann., Policy 16 (1), 55–74.

Schroedter-Homscheidt, M., Kosmale, M., Jung, S., Kleissl, J., 2018. Classifying ground-measured 1 minute temporal variability within hourly intervals for direct normal irradiances. Meteorol. Z. 27, 161–179.

Stuetzle, T., Blair, N., Mitchell, J.W., Beckman, W.A., 2004. Automatic control of a 30 MWe SEGS VI parabolic trough plant. Sol. Energy 76 (1–3), 187–193.

Wilbert, S., Nouri, B., Kötter-Orthaus, N., Hanrieder, N., Prahl, C., Kuhn, P., Zarzalejo, L. F., Lázaro, R., 2020. Irradiance Maps from a Shadow Camera on a Mountain Range. SolarPACES 2020. Online.

Wilbert, S., Nouri, B., Yasser, Z., Hirsch, T., Glumm, D., Kuhn, P., Macke, A., Noureldin, K., Schmidt, T., Schmitz, M., Schroedter-Homscheidt, M., 2018. WobaS - Wolkenkamera-basierte Betriebsstrategien für konzentrierende Solarkraftwerke.

Wittmann, M., Hirsch, T., Eck, E., 2009. Some Aspects on Parabolic Trough Field Operation with oil as a heat transfer fluid. SolarPACES, Berlin.

Zunft, S., 1995. Temperature control of a distributed collector field. Sol. Energy 55, 321–325.